Ligand Migration in Sperm Whale Myoglobin†

Emily E. Scott* and Quentin H. Gibson

Department of Biochemistry and Cell Biology, Rice University, 6100 Main Street, Houston, Texas 77005

Received March 27, 1997; Revised Manuscript Received July 17, 1997⊗

ABSTRACT: Geminate oxygen rebinding to myoglobin was followed from a few nanoseconds to a few microseconds after photolysis for more than 25 different oxymyoglobin point mutants in the presence and absence of 12 atm of xenon. In all cases, two relaxations were observed: an initial fast phase (half-time 20 ns) and a slower, smaller phase (half-time 0.5−2 μs). Generally, xenon accelerates the fast reaction but slows the slower reaction and diminishes its amplitude. The rates and proportions of the two components and the effects of xenon on them vary widely for different mutants. The locations of specific xenon binding sites [Tilton, R. F., Kuntz, I. D. Jr., and Petsko, G. A. (1984) *Biochemistry 23,* 2849−2857], the effects of point mutations on the geminate reactions, and molecular dynamics simulations were used to suggest locations in the protein interior occupied by ligands on the nanosecond to microsecond time scale. Photodissociated ligands may occupy xenon site 4 in the distal pocket and xenon site 1 below the plane of the heme. Rebinding from these positions corresponds to the slower geminate phase for O_2 rebinding. The rapid geminate component is determined by competition between rebinding from a position closer to the iron atom and escape to solvent or more distant locations in the protein.

The pathways for ligand migration from the iron atom to solvent in myoglobin have been studied intensively during the 20 years since Frauenfelder and his associates first recognized the phenomenon of geminate recombination (*1*). The methods used have included site-specific mutagenesis (*2*, *3*, *4*), time-resolved spectrophotometry (*5*, *6*, *7*), X-ray crystallography (*8*, *9*), and molecular dynamics (*10*, *11*). The results have generally agreed in suggesting that dissociated ligands initially move away from the iron and deeper into the protein to occupy a space bounded by residues F43, I107, I111, L29, V68, and H64 and the heme group, not toward the exterior (*12*). Molecular dynamics simulations and infrared spectroscopy (*5*, *6*) suggest that this movement is substantially complete within the first tens of picoseconds after dissociation. Such simulations, however, usually cover only a fraction of a nanosecond, much less than the 50 ns or so spent by a ligand molecule in the protein prior to its escape to the exterior. This raises the question of the location of ligands in this longer time frame.

One approach to this question was developed by Elber and Karplus (*10*), who used their locally enhanced sampling algorithm to follow the motions of a cloud of ligand molecules. To promote ligand escape, they increased the velocities of the ligands to the equivalent of a temperature of 3000 K. Ligands were found to occupy each of the four main xenon binding sites identified in myoglobin by X-ray crystallography (13) and to escape from the protein by a variety of routes. In a second, experimental, approach, Lim et al. (*5*, *6*) used time-resolved IR spectrophotometry to follow photodissociated CO molecules. They found that after an initial rapid movement away from the iron, the ligands appear to remain in roughly the same place until escape from the protein.

Most earlier workers have described the time course of oxygen geminate recombination to myoglobin at room temperature as a single first-order process (*14*, *15*). Chatfield et al. (*7*), however, have reported more than one nanosecond relaxation for native horse heart and sperm whale oxymyoglobins. This observation is consistent with ligands populating more than one internal site. To confirm and extend the evidence for the existence of multiple sites and to attempt their structural identification, we have examined over 25 mutant myoglobins. Since most single mutations do not disturb the general architecture of the myoglobin molecule (*3*, *24*, *26*), it may be argued that if ligands occupy specific sites during migration, only mutations near those sites will influence the nanosecond geminate reaction. Further, if such sites are related to the xenon binding sites reported by Tilton et al. (*13*), xenon and photodissociated ligands would be expected to compete to occupy them. To test these ideas, data were collected on the effects of both mutation and xenon on oxygen geminate rebinding.

MATERIALS AND METHODS

Mutants. The recombinant myoglobin mutants were constructed, expressed, and purified as described in Carver et al. (*3*), based on the original work of Springer, Sligar, and co-workers (*16*, *17*). The complete sequence of each new myoglobin gene was determined to verify the mutation and the integrity of the remaining portion of the coding region. Oxygenated proteins were prepared by the addition of dithionite to the ferric form followed by rapid passage down a Sephadex G-25 column to remove excess reducing agent (*18*). Measurements were made in 0.1 M potassium phosphate, 0.3 mM EDTA at pH 7.0 and 20 °C.

† This work was supported by Grant GM 14276 from the National Institutes of Health (Q.H.G.) and NIH Training Grant GM08280-10 (E.E.S.). United States Public Health Service Grants GM 35649 and HL 47020 (John S. Olson, Rice University) supported the construction, expression, and purification of the new mutant myoglobins used in these studies.

* Correspondence should be addressed to this author at the Department of Biochemistry and Cell Biology MS 140, 6100 Main St., Houston, TX 77005-1892. Telephone: 713-527-4861. FAX: 713-285-5154. E-mail: yertle@bioc.rice.edu.

⊗ Abstract published in *Advance ACS Abstracts,* September 1, 1997.

S0006-2960(97)00719-8 CCC: $14.00

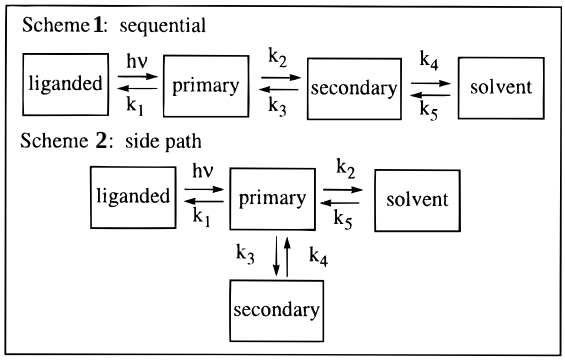

FIGURE 1: Kinetic schemes representing geminate rebinding. Liganded: MbO_2 . Primary: species giving nanosecond geminate recombination with rates k_1 and k_2. Secondary: species giving microsecond recombination through rates k_3 and k_4.

Data Collection. Time courses for oxygen geminate recombination were acquired following photolysis by a 9 ns flash at a wavelength of 532 nm from a YAG laser (Continuum Corp., Santa Clara, CA). The beam was telescoped to 3 mm and entered the 1 mm sample path normal to the cuvette. The observation beam came from a 75 W xenon arc lamp pulsed to 100−200 times normal brightness. The observing beam was collinear with the photolysis beam and about 1 mm in diameter at the cell. Observation was usually at 436 nm, near the maximum of the oxy−deoxy difference spectrum, using a combination of interference filters and a Spex 250 mm monochromator. The signals were detected with a Hamamatsu R1913 photomultiplier and recorded with a Tektronix (Beaverton, OR) 7104 oscilloscope, charge-coupled camera, and video capture board in an IBM 486 computer. A more complete description of the apparatus appears in Shibayama et al. (*19*). The combination gave about 90% photolysis of wild-type sperm whale oxymyoglobin. In most experiments, data were acquired using two time scales covering 0.8 μs and 4 μs.

For experiments with xenon, a 0.3 mL sample of MbO_2 was transferred to a stainless-steel pressure cell with a gas volume of 4 mL. The cell was equipped with 0.5 in. diameter anti-reflection coated sapphire windows and had a path length of 1 mm. Data were first collected with air in the cell. The required pressure of xenon was then introduced and the sample equilibrated with the air−xenon mixture.

Data Reduction. Data collected on two time scales were first corrected for base line drift due to variation in the output of the pulsed Xe arc. The maximum correction was under 1% of the total absorbance change measured in most experiments. Combined data from the two time scales were then fitted to the kinetic schemes in Figure 1 by nonlinear least-squares optimization. To improve the chances of locating the best solution, the minimization was repeated at least 20 times using randomly selected starting values for each of the variables optimized. It was usually possible to fit data sets with a root mean square residual less than 0.002 in absorbance or 0.5% of the total absorbance excursion, whichever was less.

It is very difficult to make valid estimates of the errors in the fitted parameters, and such errors vary greatly from mutant to mutant depending on the proportion of the reaction accounted for by each kinetic component. In favorable cases, it is estimated that the rates and amplitudes of the two geminate processes were determined with random errors less than 10%. This estimate is derived from the scatter in a series of values from experiments with xenon, and from the results of repeated experiments. In five runs with the same solution of wild-type oxymyoglobin, the range (not the standard error) lay between 5 and 8% of the mean of each of the four rate constants in Scheme 2 (Figure 1). When a separate portion of the same protein preparation was taken for each experiment, treated with dithionite, and passed through the column, the range was approximately doubled. The range of amplitudes for the total geminate reaction was 3%, and for the slower, secondary, geminate reaction was 2%. It is possible to assign so many parameters because the rates are widely different, and in the case of bimolecular rebinding the pseudo-first-order rate is low enough to be treated as a fixed correction rather than a variable. It appears that the rates and amplitudes can be assigned reliably within the limits stated.

Results with different protein preparations depended on the storage history of the sample. When samples stored in liquid N_2 were used, no difference between them could be detected. Samples stored at −70 °C, however, sometimes showed significant deviations, especially if they had been thawed and refrozen, and for that reason were not used.

A possible source of systematic error, suggested by the report of Ansari et al. (20), is that after photodissociation of CO the spectrum of deoxymyoglobin changes on a nanosecond time scale, with the major change occurring in the first 100 ns. Experiments in which the reaction of the same wild-type sample was followed at different wavelengths showed systematic changes in the amplitude of the geminate reaction consistent with their origin from deoxymyoglobin. They are seen only at wavelengths longer than isosbestic, and their relative amplitude is related to the deoxy spectrum. This effect is small at 436 nm where most measurements were made. If the reaction is followed at the maxima of the difference spectrum on either side of the isosbestic point, the differences between the data are close to the noise level of the experiments.

Molecular Dynamics. Molecular dynamics simulations were run using the program MOIL (*21*) with implementation of the locally enhanced sampling algorithm. This provides multiple copies of the ligand, each of which is influenced by the protein. The protein experiences the average forces of all ligands, which are invisible to each other. The cutoff radius for nonbonded interactions was 10 Å and the 1−4 scaling factors 2 for electrostatic and 8 for van der Waals interactions. All crystallographic water molecules (330) were included and modeled as TIP3 (*22*). The crystal structure of wild type MbO_2 (*8*) was used as a starting point, and mutations for which no crystal structures are available were prepared by truncation or exchange of the appropriate residues and energy minimization of the resulting structure. Runs with and without xenon were performed using the same distribution of initial velocities. The temperature of the protein was raised to room temperature over the first 15 ps.

Scheme for Representation of Data. Two schemes, termed sequential and side path, have been applied extensively to interpret the data and are shown in Figure 1. In each case, computation begins with the protein in the liganded form. Photodissociation of the ligand generates a product called the primary species in both schemes. In the sequential model (Scheme 1), the primary product disappears by return to the liganded form (k_1) or by conversion to the secondary species

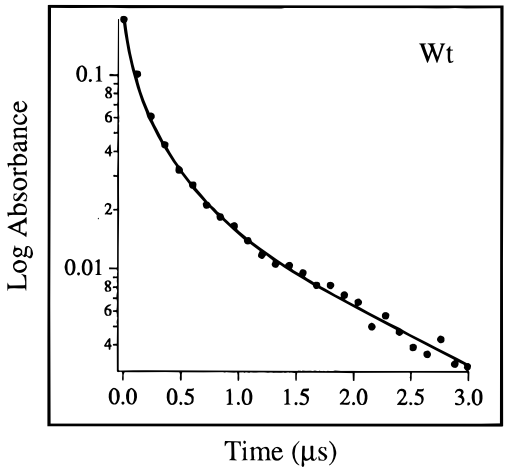

FIGURE 2: Semi-log plot of oxygen rebinding to sperm whale myoglobin following photolysis. The bimolecular contribution to rebinding kinetics has been subtracted. The two rates required are 6.3×10^6 s^{-1} and 8×10^5 s^{-1}.

(k_2). In turn, the secondary species may re-form the primary product (k_3) or escape to solution (k_4). In the side path model (Scheme 2), escape to the exterior is from the primary species only (k_2). The secondary species is formed from the primary species (k_3) and returns to the primary species only (k_4). In both models, the bimolecular reaction occurs between the protein and ligands in solution (k_5) to form either the secondary species (Scheme 1) or the primary species (Scheme 2).

Numerically, both schemes yield equally good fits to the data. However, the effects of xenon on the fraction of geminate rebinding and the rate of escape presented here strongly support the side path scheme as a more structurally plausible model. In the sequential model, xenon would fill internal spaces on the escape route. Consequently, the fraction of geminate rebinding would be expected to increase and the escape rate to decrease. The opposite is observed experimentally. The addition of xenon results in no change in the fraction and an increase in the rate of geminate escape. Both of these effects are predicted by the side path model which implies that escape does not occur through channels where xenon occupancy is allowed. In our view, the side path model is the more plausible, and consequently only parameters from Scheme 2 are reported. Chatfield et al. (*7*) also examined the two models in great detail and discarded the sequential model in favor of a side path model.

RESULTS AND DISCUSSION

General Scheme. The results for wild-type sperm whale myoglobin (Figure 2), in agreement with those of Chatfield et al. (*7*) for native sperm whale myoglobin, show two well-separated kinetic components. If interpreted in structural terms, such data require at least two sites from which ligands return to the iron at widely different rates. The three most effective indicators of ligand position are site-directed mutagenesis, X-ray crystallography, and molecular dynamics simulation. These suggest that (viewing native myoglobin in the same orientation as in Figure 8) ligand molecules move toward the interior of the protein and upward to a position about 5 Å from the heme iron [toward residues L29 and I107 and xenon site 4 of Tilton et al. (*13*)] in the first few picoseconds following dissociation. The ligands return to

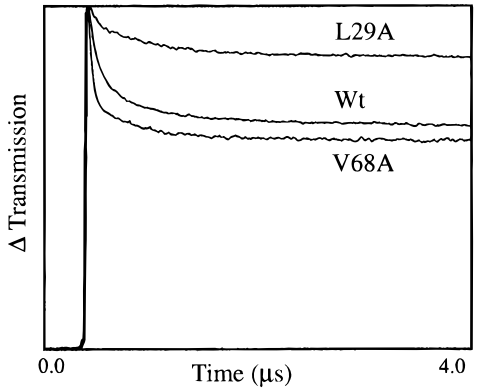

FIGURE 3: Geminate rebinding of oxygen to L29A, wild type (wt), and V68A sperm whale myoglobin mutants. The ordinate is the change in transmission. The traces begin before the photolysis flash and continue for 4 μs. The excursions have been scaled, but are uncorrected.

the neighborhood of the heme iron either to be recaptured or to escape through the histidine gate of Case and Karplus (*23*). This process, here called primary recombination, is described by k_1 and k_2 in the kinetic scheme and has a half-time of some 20 ns. Other ligand molecules move to xenon site 4 (defined by G25, I28, L29, V68, and I107) or around the edge of the heme and appear below the heme plane in the xenon 1 site (defined by L89, H93, L104, and F138) of Tilton et al. (*13*). These molecules may return to the neighborhood of the iron and be recaptured, giving rise to the contribution to rebinding defined by rates k_3 and k_4 in the scheme, here called secondary recombination. This description derives from the work of many authors and is consistent with the recent review of Olson and Phillips (*12*).

Experimental data of the type shown in Figure 3 are sufficient to determine all four geminate rates in Scheme 2 of Figure 1. Rates k_1 and k_2 are constrained by the rate and amplitude of the primary (rapid) geminate reaction. Their sum must be of the same order as the rate constant which would be assigned if the data were fit to a single exponential and a constant while their ratio is determined by the amplitude of the primary geminate reaction. The relation between rates k_3 and k_4 and the extent of observed rebinding in the secondary phase is more complex because all four rate constants contribute to the amplitude and rate of disappearance of the secondary intermediate. Ligands that return to the primary species through k_4 are repartitioned by operation of rates k_1, k_2, and k_3. The result is that k_4 must be higher than the observed rate constant for the slower geminate phase.

To facilitate comparison between many mutants in the presence and absence of xenon, we have used the maximum population of the secondary species during rebinding. This value is determined by using the fitted rate parameters (k_1–k_4) and the rate equations presented by Scheme 2 (Figure 1) to calculate the population of the secondary species as a function of time. The maximum population of the secondary species is expressed as a percentage of the geminate (denoted as max % 2^{nd} in the tables and figures) to afford a convenient measure of its relative significance in the geminate phenomenon. Numerical values for the rates constants, the percent geminate recombination, and the maximum percentage of

Table 1: Rates 1−4 ($\times 10^{-6}$ s^{-1}), Percent Total Geminate, and Percent Secondary Species in the Presence and Absence of Xenon for the Myoglobin Mutants Examined Calculated Using Scheme 2[a]

	air						xenon (12 atm)					
mutant	k_1	k_2	k_3	k_4	% total geminate	max % 2nd species[b]	k_1	k_2	k_3	k_4	% total geminate	max % 2nd species[b]
wt	5.30	6.10	3.90	2.70	42	20	6.62	7.47	1.06	1.75	40	6
L29A	1.69	7.62	8.19	2.93	16	36	5.41	12.60	2.93	0.73	24	11
L32A	4.24	7.73	6.15	3.37	30	26	5.24	10.70	2.74	1.54	27	13
L32V	3.28	6.27	2.63	2.78	30	15	4.41	9.38	1.52	0.56	26	10
L32I	5.52	8.02	3.34	3.16	36	15	4.76	10.70	1.36	0.99	25	7
L32F	6.00	6.94	2.49	3.20	41	12	5.48	8.99	1.35	1.27	33	8
L32M	7.62	8.55	4.04	2.94	41	16	10.70	8.98	1.48	2.17	48	6
L32W	19.40	15.50	3.09	3.26	46	8	22.00	16.00	1.02	1.40	47	3
F43V[c]	(0.4)	(12)	ND	ND	3	0	(0.2)	(20)	ND	ND	1	0
F46V[c]	(0.70)	(4.60)	ND	ND	12	0	(1.3)	(6.9)	ND	ND	14	0
V68A	14.90	14.80	4.70	2.77	41	13	21.20	17.00	2.74	12.40	45	5
L104A	4.55	4.79	4.72	4.49	45	22	13.90	10.50	1.40	1.25	49	6
L104V	8.11	8.49	3.71	2.63	43	15	11.00	8.63	1.43	1.26	50	7
L104W	13.40	9.31	1.80	3.47	52	6	16.00	11.50	1.25	1.48	50	5
I107A	3.14	4.95	3.55	4.00	36	19	4.15	10.20	1.02	1.02	24	6
I107V	2.78	5.12	2.61	2.03	33	18	1.77	8.06	3.41	0.73	15	23
I107L	2.97	5.33	3.48	2.25	33	22	2.50	6.95	2.00	1.02	23	15
I107W	26.30	13.2	3.07	3.25	55	8	22.00	17.90	2.54	2.22	44	6
I111V	4.66	5.95	3.64	3.72	40	18	6.94	7.17	1.87	1.25	43	11
I111F	3.30	4.85	2.70	2.66	37	17	7.56	6.28	1.09	1.34	48	7
I111M	8.21	11.00	8.98	5.62	36	26	7.50	6.78	1.43	1.02	47	8
I111L	3.77	6.26	3.45	4.29	34	18	7.43	6.55	0.91	1.33	47	5
I111W	7.28	6.92	4.46	4.84	46	17	11	8.32	1.53	0.81	49	8
F138A	3.52	3.59	2.45	3.62	47	16	8.18	7.13	1.21	2.04	48	6
F138W	5.71	8.65	1.75	2.04	35	9	7.66	8.58	0.77	1.96	40	4

[a] The rates are given to two decimal places to permit their use in reproducing the experimental results. Percentage total geminate and secondary species (% 2nd) refer to the total absorbance excursion. [b] The fitted rates presented here are used to calculate the population of each species as a function of time using Scheme 2. The maximum population of the secondary species expressed as a percentage of the geminate reaction (max % 2nd species) is given to facilitate comparison of its significance for different mutants. [c] The overall geminate amplitudes for the position 43 and 46 mutants were so small that analysis in terms of two phases was not possible.

the second species are presented for all of the mutants in Table 1.

Effects of Mutation and Xenon. Scheme 2 has been used to describe the effects of both mutation and xenon on geminate recombination. Mutation may be expected to affect both the rapid and slow phases of geminate recombination by changing the volume accessible to diffusing ligands or by affecting barriers to exit from the protein. Xenon may be expected to influence nanosecond recombination by occupying site 4 in the distal pocket and site 1 below the heme (*13*), thereby limiting their occupancy by ligands. The result should be faster and more extensive rapid nanosecond recombination (k_1 and k_2), as is observed for wild-type sperm whale myoglobin and all of the mutants examined. The amplitude and rate of the secondary geminate reaction are more sensitive to xenon than the primary reaction, with a decrease in the peak population of the secondary species and slowing of the reaction by a factor of approximately 2 in experiments with 12 atm of xenon.

As crystallography has suggested that xenon site 1 is populated some 10 times more readily than site 4 (13), the contributions of xenon sites 1 and 4 may, in principle, be distinguished by varying the partial pressure of xenon. Progressive changes in recombination for wild type are observed as the pressure is increased (Figure 4), and the effects of xenon on the four kinetic parameters and on the peak population of the secondary species are presented in Figure 5. For wild-type sperm whale myoglobin, rates k_1 and k_2 increase in parallel by some 30% and, within error, linearly with xenon partial pressure. Rate k_4 decreases moderately, again linearly, while k_3 and the peak population of the secondary species decrease nonlinearly by 70% and are closely correlated. The changes in the population of the secondary site are consistent with its occupation by a xenon molecule requiring about 3 atm of xenon for half-saturation. Even at the highest pressures, some secondary reaction remains, perhaps implying another site inaccessible to xenon.

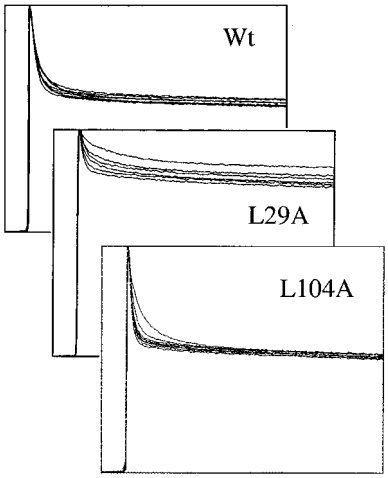

FIGURE 4: Reaction records for wild type, L29A, and L104A myoglobin in the presence of increasing partial pressures of Xe. The data are presented as changes in percentage transmission and have not been corrected for base line fluctuation. The increments in xenon pressure vary between the mutants but were usually approximately 1.2 atm below 8 atm and 2.5 atm at the higher pressures. In all cases, the lowest xenon pressure gives rise to the uppermost trace and the highest xenon pressure (12 atm) gives the lowest trace.

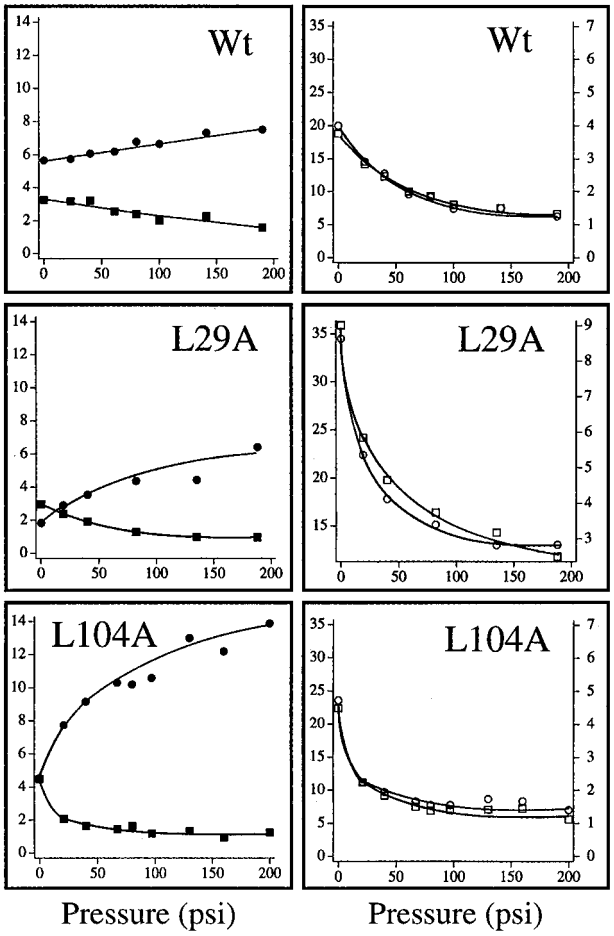

FIGURE 5: Rates k_1, k_3, and k_4 and maximum percentage of the secondary species (as determined by using the fitted rates) for wild type, L29A, and L104A at increasing partial pressures of xenon. The rates are in units of 10^6 s^{-1}. Closed circles, k_1; closed squares, k_4; open circles, k_3; open squares, maximum percent secondary species.

Table 2: Summary of Mutants Showing the Percentage Total Geminate and Maximum Percentage Secondary Species in the Presence and Absence of Xenon Calculated Using Scheme 2[a]

	air		xenon (12 atm)	
mutant	% total geminate	max % 2nd species	% total geminate	max % 2nd species
wt	42	20	40	6
L29A	16	36	24	11
V68A	41	13	45	5
L104A	45	22	49	6
L104W	52	6	50	5

[a] Percentage total geminate and secondary species (max % 2nd) refer to the total absorbance excursion.

Examination of mutants suggests that the residues at positions 29, 68, 43, 46, and 104 are important determinants of oxygen geminate rebinding. In the mutant L29A, the increased space accessible to the ligands may be regarded as augmenting xenon site 4. In the absence of xenon, the amplitude of the rapid geminate reaction is less than that of wild type (Figure 3, Table 2). This is due to a 70% decrease in k_1 (rapid recombination) associated with an increased ligand accessible volume (Figure 6). The relatively small overall geminate amplitude requires, further, that the sum of rates k_2 and k_3 (escape from the iron) be large compared with k_1 (fast rebinding). As a result, the weighting of the

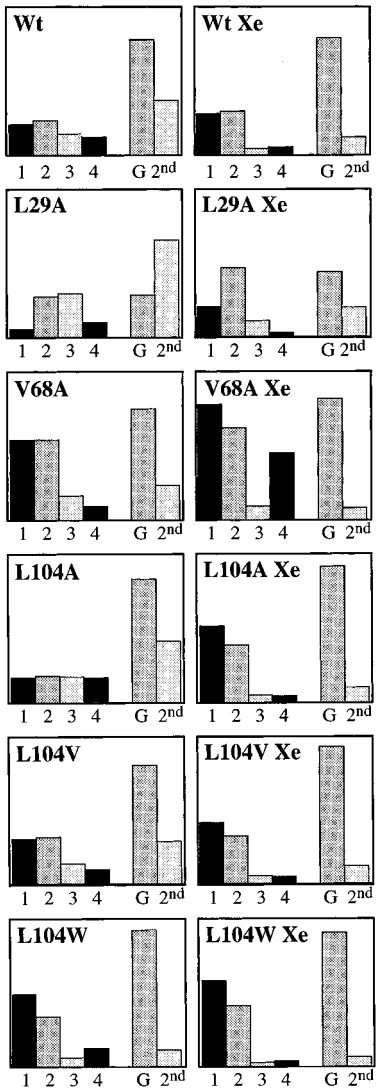

FIGURE 6: Profiles showing rates k_1-k_4 (*1*−*4*), geminate rebinding as a fraction of the total absorbance change following photolysis (G), and the proportion of absorbance change attributable to the secondary species (2nd) using Scheme 2 (Figure 1) for the mutations indicated, in the presence and absence of 12 atm of Xe. The same scale is used for all rates with a range of $(0-25) \times 10^6$ s^{-1}. The range for the overall geminate reaction (G) and for the secondary reaction (2nd) is 0−50%.

secondary site in determining the geminate kinetics is largely increased. A large population of the secondary site is compatible with the moderate amplitude of the observed secondary reaction because returning ligands are more likely to escape to the exterior than to be recaptured by the iron (small k_1). Xenon fills the space created by the L29A mutation to return the parameters toward those observed for wild type (Figure 6). The behavior of wild type and L29A as a function of xenon partial pressure is shown in Figure 5. As with the wild type, there is a progressive change in the kinetic parameters and populations of the species which continues to the highest pressure of xenon used, a result consistent with an important role for the low-affinity xenon site 4.

The mutation V68A was expected to resemble L29A because the new space created should also communicate with xenon site 4. However, the experimental results for V68A are significantly different from those for L29A, as shown in

Figure 3 which compares observed rebinding for the two mutants. The contribution of the primary reaction is much larger for V68A while the secondary reaction is more like that of wild type than that of L29A. The corresponding rate parameters (Figure 6, Table 2) show much higher values for rates k_1 and k_2. The addition of xenon further increases rates k_1 and k_2 while sharply increasing k_4, leading to the effective disappearance of the secondary species. Although the new space created by the V68A mutation is near xenon site 4, site 4 is apparently not readily accessible to ligands. These results are similar to those reported by Quillin et al. (*24*) who found an increased oxygen bimolecular rate and a faster nanosecond geminate rate for this mutant.

Substitutions at positions 43 and 46 have marked effects, decreasing the amplitude of the total geminate reaction so much that analysis into multiple components is difficult and only the values of k_1 and k_2 were determined. Primary rebinding is much slower in F43V and F46V than in other mutants, but the rate of escape (k_2) remains normal. The effect is that the total amplitude for geminate rebinding decreases with little change in the half-time of the process. Lai et al. (*26*) reported similar oxygen rebinding for F46V. Xenon has little effect on either the rate or the amplitude of geminate recombination of F43V and F46V mutants. These results are consistent with the suggestion of Lai et al. (*26*) that ligands move directly to solvent through the histidine gate without migrating into the protein interior.

Data are available for three mutants at position 104, which is on the proximal side of the heme and lies between xenon sites 1 and 2 of Tilton et al. (*13*). The mutation L104A gave comparatively low values for all 4 rate constants, and its geminate reaction has the largest proportion of secondary recombination in our series (Table 2, Figure 6). The effect of Xe has been studied as a function of partial pressure and shows a large step in the rates and proportions of the reactions, with pressures as low as 1 atm accounting for most of the effect observed (Figures 4 and 5). As with other mutants, the rate of primary recombination is increased and the proportion of secondary recombination decreased by Xe. These effects are consistent with an augmented role of Xe site 1 in this mutant, presumably due to the increase in the volume available to it. The increase in the rates k_1 and k_2 on the addition of xenon is larger than usual in this mutant and does not seem to have an obvious explanation. The second mutant L104V has not been studied in as much detail as L104A, but is closer to the wild type in its behavior (Figure 6).

The third mutant, L104W, shows rapid primary recombination with little secondary reaction (Figure 6). The effect of Xe is slight but in the same sense as with the other mutants, speeding primary recombination and reducing secondary recombination. Taken together, the results with these three mutants are readily explained in terms of kinetic Scheme 2 by assuming that Xe site 1 is a significant secondary site. The L104A substitution increases its role, which, however, is reversed by Xe even at low pressures, generating the initial step in the experiment of Figure 5. The substitution L104W has the opposite effect, cutting down the role of Xe site 1, perhaps by filling the site itself. If so, the effect of Xe on the reactions would be much reduced, as was observed experimentally.

A considerable group of distal mutations remote from the iron (L32A, L32V, L32M, I107A, I107L, I111V, I111L, I111F, I111M, and I111W) and F138A on the proximal side show behavior similar to that of wild-type oxymyoglobin. The parameters for these mutants are summarized in Figure 7. Substitution of Trp at these positions, however, produces significant, and often large, effects on the geminate rate parameters.

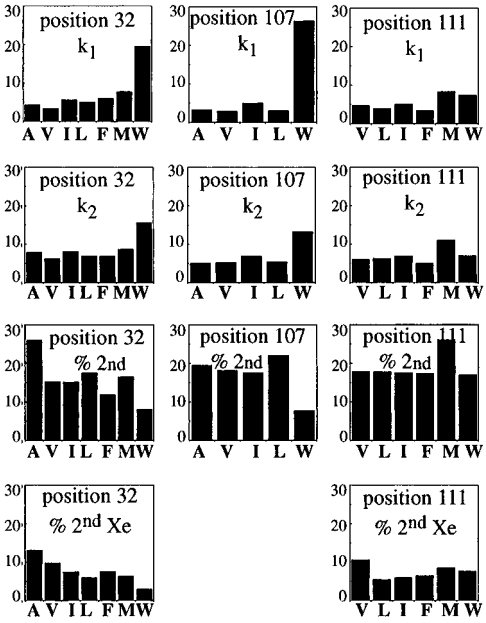

FIGURE 7: Rates k_1 and k_2 and the maximum % 2nd species in the presence and absence of Xe for the mutations shown at positions 32, 107, and 111. The rates run from 0 to 30×10^6 s^{-1}. Maximum % 2nd species is the maximum population of the secondary species obtained by using the fitted rate constants to calculate the populations of each species in Scheme 2 and is shown as a percentage of the total absorbance change following photolysis.

Six substituents for L32 have been examined; they are A, V, I, F, M, and W. The results shown in Figure 7 form a regular series with k_1 (primary rebinding) and k_2 (escape) both rising as the bulk of the substituent increases, consistent with a decrease in the volume accessible to ligands. In effect, the activity of the ligand in the cavity is increased when its volume is decreased, promoting both recombination and escape. At the same time, there is an inverse relation between the size of substituent and the amplitude of secondary rebinding, larger free space affording more extensive and longer lasting accommodation for ligand molecules relatively far from the iron. Thus, for L32A secondary rebinding accounts for 26% of the total amplitude of the reaction, decreasing to 8% for L32W. The effect of Xe on this series of mutants is relatively modest with 12 atm of Xe decreasing secondary rebinding of L32A from 26 to 15%, and of L32W from 8% to 3%.

Analogous considerations apply to substitutions at position 107 (Figure 7), but the effects are smaller except for I107W where the substitution increases the rate of primary rebinding 7-fold as compared with I107A and reduces the proportion of secondary rebinding from 20% to 8%. Xenon has relatively small effects on these rates and reduces the proportions of secondary rebinding to 13% and 6.5%, respectively.

The effects of substitution at position 111 are smaller still (Figure 7). The primary rates (rates k_1 and k_2) for I111V and I111W differ by less than 50%, and there are only small increases with 12 atm of Xe. The peak population of the

secondary species is the same as that for wild type, and drops uniformly for all residue sizes to the same extent as wild type. Evidently the volume changes associated with these substitutions are in locations which are not readily accessible to ligands in wild type and so do not influence the reactions.

Molecular Dynamics. Lim et al. (*5*, *6*) reported that CO molecules do not move far from the positions assumed soon (i.e., picoseconds) after photodissociation. If so, there might be a correlation between molecular dynamics simulations (picoseconds) and primary and secondary geminate recombination (nanoseconds to microseconds). In selecting residues for detailed consideration, only primary recombination is relevant because the time scale for loading and unloading a secondary site is likely to be far beyond the range of molecular dynamics simulations. Further, proximal substitutions cannot be expected to produce meaningful results on the simulation time scale leaving L29, V68, F43, and F46 as prime candidates.

Simulations of diffusion in L29A have already been reported (25) and show rapid movement of ligand molecules to a large space above the heme bounded by G25, A29, F43, G65, V68, and I107. There were few returns from this space to the region of the heme iron. This has been confirmed in new simulations, for example, panel 1 (top) of Figure 8 where there were only two returns to within 4 Å of the iron in 50 ps of simulation. In a run with xenon atoms in sites 1−4 (13) but which was otherwise identical, including the initial distribution of velocities, the ligands were held much closer to the iron (panel 2, middle, Figure 8), and there were 456 close approaches of ligand atoms to the iron. The number of close approaches varied unusually widely in other runs with xenon, depending on the exact position assumed by the xenon atom which sometimes allowed the ligand molecules to pass into a large space far from the iron. The low was 16 approaches and the high 731 out of 1000 possible. This result corresponds qualitatively, but not quantitatively, to the L29A data for k_1 presented here.

The mutant V68A might be expected to give similar results to L29A, but does not do so either in the simulations reported by Quillin et al. (24) or in confirmatory simulations undertaken here. Both show large numbers of returns of ligands to the neighborhood of the iron atom. Introduction of xenon caused little change in the position of the ligands which were held near the iron below xenon 4 in all cases, giving large, relatively uniform, numbers of returns of ligand atoms to within the reaction radius of the iron. This result agrees with experiment to the extent that the value for k_1 is among the largest found among the mutants examined, and is some 8 times larger than that for L29A. It is also unusual in being unaffected by 12 atm of xenon. The position taken up by the ligands in the presence of xenon is shown in panel 3, bottom, of Figure 8. It seems that the nanosecond experiment and picosecond simulation show some parallelism for V68A also.

The behavior of mutants at positions F43 and F46, as already mentioned, is quite different from the other mutants studied in that geminate recombination is minimal. Mutations at position 46 have been examined by Lai et al. (*26*), who reported simulations showing that ligands leave the vicinity of the iron traveling toward positions 64 and 46, i.e., in the opposite direction to that usually observed. In mutations such as F46V, the reduction in size of the residue is accompanied by apparent opening of a channel, allowing ligands to pass H64 and escape to the solvent. Again, this behavior corresponds to the observed nanosecond recombination results which require small values of k_1 and large values of k_2.

Simulations of ligand diffusion in mutations at I107, in contrast, do not show a good correlation with experiment. As shown in Figure 7, rates k_1 and k_2 are small for all mutations except I107W and are the same within experimental error. Simulations, however, show large differences in the numbers of returns to the iron atom depending on the size of the substituent, with I107A showing essentially no returns, while I107L and I107F give moderate and very large numbers of returns, respectively.

Very recently, the first time-resolved crystallographic data have shown CO molecules, 4 ns after photodissociation, in or around xenon site 4, which had disappeared after 1 μs (27). This result is consistent with our experiments since, although there should be a peak population of about 15−20% at the secondary site, for native sperm whale myoglobin, this should have declined to some 5% or so at 1 μs, well below the level of X-ray detection. Ligand molecules in the primary site should have escaped to solution with a half-time of 40 ns, and would also be invisible. As mentioned previously, the applicability of alternative, usually sequential, models, though not favored, remains open. The sequential and side path models require widely different distributions of species. In particular, the sequential model calls for much higher populations of secondary species. This suggests that the models might be distinguished by kinetic crystallography, particularly using mutants with markedly different kinetic behavior.

Observations of polarization have led Lim et al. (5, 6) to conclude that carbon monoxide molecules occupy, and remain oriented in, a docking site for at least 0.1 ns after dissociation. Molecular dynamics simulations suggest that this site is similar in all of the mutants so far examined, with the exception of mutations at positions F43 and F46. It is proposed that the faster nanosecond (primary) recombination takes place from this docking site. The slower (secondary) recombination arises from migration of ligands to locations more remote from the heme, followed by a return to the docking site and recapture by the iron. The X-ray data of Tilton et al. (13) together with nanosecond recombination data for mutants and molecular dynamics simulations suggest that the secondary ligand sites include xenon site 1, defined by L89, A90, H93, L104, F138, and I142, and xenon site 4, defined by G25, I28, L29, V68, and I107. The proximal xenon site 1 is particularly implicated by the results with the mutants L104A and L104W. The mutant L104A shows behavior corresponding to a large population of the secondary site by ligands, which is readily reversed by small partial pressures of xenon, consistent with the high occupancy of this site reported by Tilton et al. (*13*). The L104W mutant behaves as though the aromatic residue occupies xenon site 1. As the fraction of geminate recombination is only slightly increased in experiments with high partial pressures of xenon, it is unlikely that these xenon sites are on the escape route. This favors, by exclusion, the classical proposal of escape through the histidine gate suggested in 1979 by Case and Karplus (*23*).

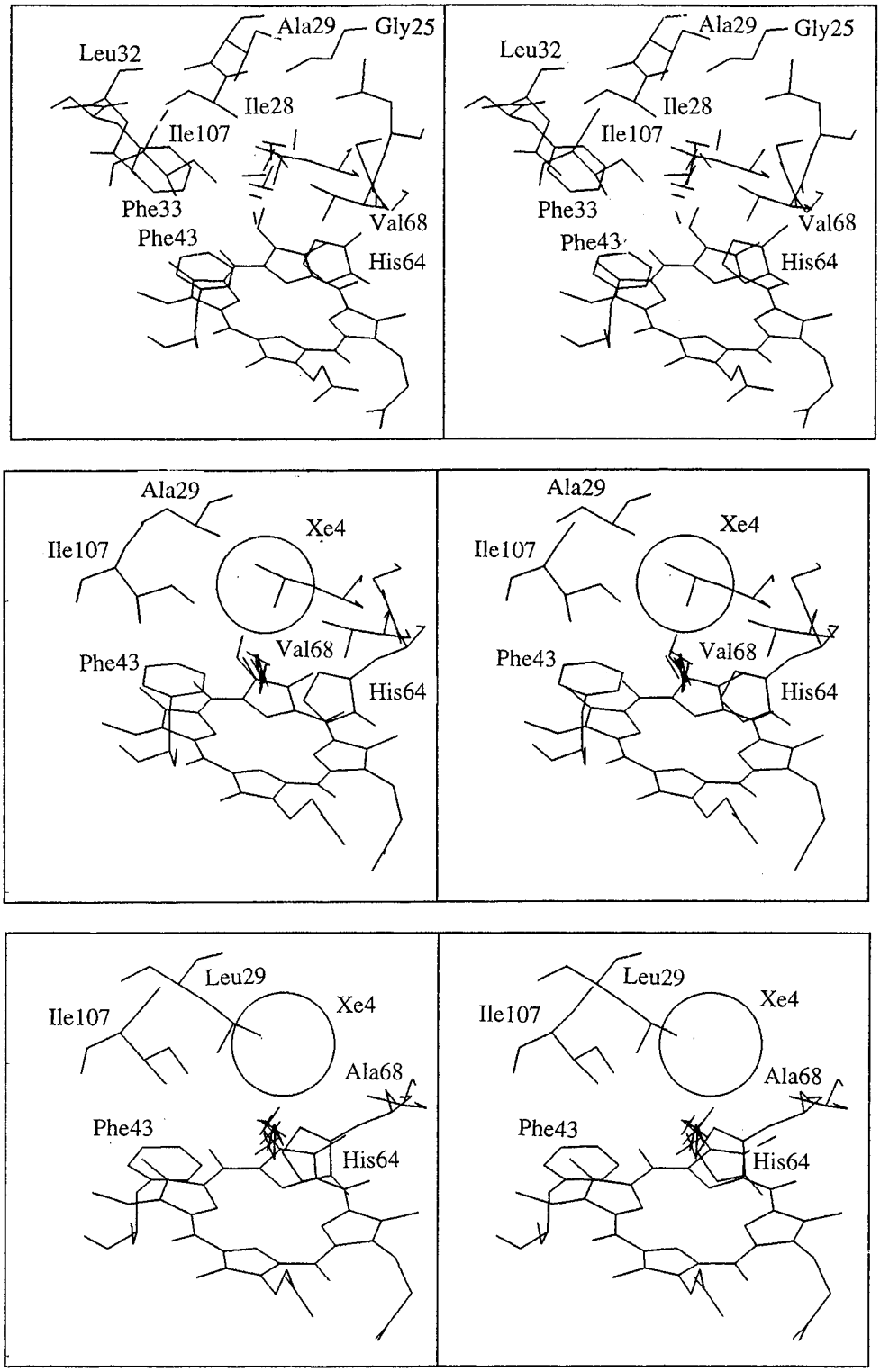

FIGURE 8: Stereo stick diagrams showing residues closely approached by a ligand molecule during molecular dynamics simulations. Panel 1 (top) is L29A without xenon. The frame is taken early in the simulation and shows ligands in transit into xenon site 4 . Residues left unlabeled are L61, G65, and L69. Panel 2 (middle) is L29A with xenon atoms in positions 1−4 (*13*). Residues unlabeled are L61 and G65. Panel 3 (bottom) is V68A with xenon.

ACKNOWLEDGMENT

We thank Eileen W. Singleton for purifying the recombinant proteins used in these studies and constructing the new single mutants at positions 32, 104, 107, and 111. It is evident that the work described here was only possible because of our access to a library of sperm whale mutants built up by Dr. J. S. Olson and his associates at Rice University. We are also indebted to Dr. Olson for his interest in the project and for many helpful discussions.

REFERENCES

1. Austin, R. H., Beeson, K. W., Eisenstein, L., Frauenfelder, H., and Gunsalus, I. C. (1975) *Biochemistry 14*, 5355−5373.
2. Springer, B. A., Sligar, S. G., Olson, J. S., and Phillips, G. N., Jr. (1994) *Chem. Rev. 94*, 699−714.

3. Carver, T. E., Brantley, R. E., Jr., Singleton, E. W., Arduini, R. M., Quillin, M. L., Phillips, G. N., Jr., and Olson, J. S. (1992) *J. Biol. Chem. 267*, 14443−14450.
4. Lambright, T. G., Balasubramanian, S., Decatur, S. M., and Boxer, S. G. (1994) *Biochemistry 33*, 5518−5525.
5. Lim, M., Jackson, T. A., and Anfinrud, P. A. (1995a) *J. Chem. Phys. 102*, 4355−4366.
6. Lim, M., Jackson, T. S., and Anfinrud, P. A. (1995b) *Scienc*e 269, 962−966.
7. Chatfield, M. D., Walda, K. N., and Magde, D. (1990) *J. Am. Chem. Soc. 112*, 4680−4687.
8. Phillips, G. N., Jr. (1990) *Biophys. J. 57*, 381−383.
9. Phillips, G. N., Jr., Arduini, R. N., Springer, B. A., and Sligar, S. G. (1990) *Proteins: Struct., Funct., Genet. 7*, 358−365.
10. Elber, R., and Karplus, M. (1990) *J. Am. Chem. Soc. 112*, 9161−9175.
11. Carlson, M. L., Regan, R. M., and Gibson, Q. H. (1996) *Biochemistry 35*, 1125−1136.
12. Olson, J. S., and Phillips, G. N., Jr. (1996) *J. Biol. Chem. 271*, 17593−17596.
13. Tilton, R. F., Kuntz, I. D., Jr., and Petsko, G. A. (1984) *Biochemistry 23*, 2849−2857.
14. Gibson, Q. H., Olson, J. S., McKinnie, R. E., and Rohlfs, J. (1986) *J. Biol. Chem. 261*, 10228−10239.
15. Carver, T. E., Rohlfs, R. J., Olson, J. S., Gibson, Q. H., Blackmore, R. S., Springer, B. A., and Sligar, S. G. (1990) *J. Biol. Chem. 265*, 20007−20020.
16. Springer, B. A., and Sligar, S. G. (1987) *Proc. Natl. Acad. Sci. U.S.A. 84*, 8961−8965.
17. Egeberg, K. D., Springer, B. A., Sligar, S. G., Carver, T. E., Rohlfs, R. J., and Olson, J. S. (1990) *J. Biol. Chem. 265*, 11788−11795.
18. Rohlfs, R. J., Matthews, A. J., Carver, T. E., Olson, J. S., Springer, B. A., Egberg, K. D., and Sligar, S. G. (1990) *J. Biol. Chem. 265*, 3168−3176.
19. Shibayama, N., Yonetani, T., Regan, R. M., and Gibson, Q. H. (1995) *Biochemistry 34*, 14658−14667.
20. Ansari, A., Jones, C. M., Henry, E. R., Hofrichter, J., and Eaton, W. A. (1994) *Biochemistry 33*, 5128−5145.
21. Elber, R., Roitberg, A., Simmerling, C., Goldstein, R. F., Verkhiver, G., Li, H., and Ulitsky, A. (1994) in *Statistical mechanics, protein structure and protein substrate interactions* (Doniach, S., Ed.) Plenum Press, New York, New York.
22. Jorgensen, W. L., Chandrasekhar, J., and Madura, J. D. (1983) *J. Chem. Phys. 79*, 7270−7286.
23. Case, P. A., and Karplus, M. (1979) *J. Mol. Biol. 132*, 343−368.
24. Quillin, M. L., Li, T., Olson, J. S., Phillips, G. N., Jr., Dou, Y., Ikeda-Saito, M., Regan, R., Carlson, M., Gibson, Q. H., Li, H., and Elber, R. (1995) *J. Mol. Biol. 245*, 416−436.
25. Gibson, Q. H., Regan, R., Elber, R., Olson, J. S., and Carver, T. E. (1992*) J. Mol. Chem. 267*, 22022−22034.
26. Lai, H. H., Li, T., Lyons, D. S., Phillips, G. N., Jr., Olson, J. S., and Gibson, Q. H. (1995) *Proteins: Stuct., Funct., Genet. 22*, 322−339.
27. Srajer, V., Teng, T., Ursby, T., Pradervand, C., Ren, Z., Adachi, S., Schildkamp, W., Bourgeois, M., Wulff, M., and Moffat, K. (1996) *Science 274*, 1726−1729.

BI970719S